Tribology and Materials
Vol. 5, No. 1, 2026, pp. 22-30

ISSN 2812-9717
https://doi.org/10.46793/tribomat.2026.005

Anodic and chrome coatings for firearm barrels: Microstructural and phase analysis

Veselina DIMITROVA [1], Ventsislav DIMITROV [1,*], Galya ZDRAVCHEVA [2]

[1] Faculty of Engineering and Pedagogy of Sliven, Technical University of Sofia, Sliven, Bulgaria
[2] Technical College – Sofia, Technical University of Sofia, Sofia, Bulgaria
*Corresponding author: vpdd_acad@tu-sofia.bg

Keywords
electrochemical rifling
firearm barrel
chromium coatings
aluminium oxide
XRD
EDS
surface characterisation
military coatings

History
Received: 01-09-2025
Revised: 08-10-2025
Accepted: 29-11-2025

Abstract

The study employs X-ray diffraction (XRD), energy-dispersive X-ray spectroscopy (EDS) and metallographic analysis to assess the phase composition and microstructural features of anodic and chrome coatings. In response to increasing demands for enhanced durability and corrosion resistance in defence applications, surface treatments have become an integral part of the barrel manufacturing process. Aluminium barrels were anodised, while steel barrels were hard chrome plated. The electrochemical rifling (ECR) process was conducted under optimised conditions: current ≈ 950 A, voltage ≈ 7 V, pressure ≈ 2.2 MPa and duration ≈ 176 s. Before coating deposition, the inner bore surface roughness was controlled at *Ra* = 0.8 μm, ensuring reliable adhesion of the subsequent layers. The XRD and EDS results confirmed near-stoichiometric compositions for both coating types. The anodised layers revealed aluminium and γ-Al_2O_3 phases, accompanied by minor intermetallic compounds, such as S (Al_2CuMg), T ($Al_2Mg_3Zn_3$) and η ($MgZn_2$). Chrome-plated steel sample exhibited the presence of elemental chromium and goethite (β-FeOOH). These findings support the suitability of the ECR method as a foundation for high-performance coating systems in military applications.

1. Introduction

Anodic oxidation, commonly referred to as anodising, is a proven technique for forming a thick, porous oxide layer on aluminium surfaces. This surface layer provides improved corrosion resistance and significantly increases the adhesion strength of any subsequent coating systems applied to the alloy [1].

The process involves an electrochemical reaction in which the aluminium substrate serves as the anode in an electrolytic cell. Under the influence of an applied current and in a suitable electrolyte, a layer of anodic aluminium oxide forms on the surface [2]. These pores can be tailored in terms of diameter and spacing depending on the operating conditions [3,4], making anodised surfaces suitable for advanced engineering applications, especially in protective coatings and micro-scale surface engineering. Anodic aluminium oxide formed by porous-type anodisation under a controlled electrochemical condition is characterised by a large number of non-interconnecting parallel pores extending through the film to the oxide/metal interfaces [5], where each cylindrical nanopore is closed by a thin barrier oxide layer with hemispherical geometry [6,7].

Chromium coatings are well known for their exceptional mechanical and tribological performance, exhibiting high hardness levels (typically in the range of 600 – 900 HV), excellent resistance to wear and elevated temperatures and a low coefficient of friction, often two to three times lower than that of conventional steel surfaces [8,9].

The electrodeposition mechanism of chromium is notably complex, involving several simultaneous electrochemical reactions at the cathode during the plating process [10]. These include: chromium

deposition; hydrogen evolution; reduction of hexavalent chromium to trivalent and elemental chromium; at the same time, a thin surface film forms on the cathode, comprising reduction by-products of chromic acid and associated anionic species.

In practical applications, standard sulphate-based electrolytes are typically employed. These contain chromic acids (H_2CrO_4 and $H_2Cr_2O_7$), sulfuric acid (providing SO_4^{2-} anions) and trivalent chromium species. Typical operating parameters include a current density of 30 – 60 A/dm^2 and a temperature range of 45 – 70 °C. However, such electrolytes are associated with low current efficiency and moderate coating hardness [11].

Chromium coatings inherently exhibit high internal stresses, primarily attributed to the spontaneous transformation of the metastable β-Cr phase to the thermodynamically stable α-Cr phase, which has a higher density. This phase transition leads to the development of a network of microcracks within the deposited layer. Notably, increasing electrolyte temperature has been shown to reduce both the magnitude of internal stresses and the prevalence of microcracking.

2. Materials and methods

The experimental investigations were carried out on real under-barrel grenade launcher barrels. The rifling of the barrel is achieved through the electrochemical rifling (ECR) process [12,13], performed under controlled parameters: current ≈ 950 A, voltage ≈ 7 V, pressure ≈ 2.2 MPa and processing time ≈ 176 s. The resulting internal surface quality is evaluated by surface roughness, specifically the arithmetic mean deviation of the profile, with a target value of *Ra* = 0.8 µm, which is considered a critical threshold for subsequent coating adhesion [14-16].

The chemical composition and mechanical properties of the barrel materials produced by the ECR process correspond to aluminium alloy EN AW-7075 (EN 573-3) and steel 30CrNiMo8 (EN 10083-3). These materials are compatible with surface modification through anodising and hard chrome plating, both of which have been validated as suitable for firearm barrels [17,18]. The two types of coatings were deposited under distinct technological regimes. For the hard anodising process, the barrels were treated under the following operating conditions and electrolyte composition: sulfuric acid (H_2SO_4) of 150 – 200 g/l; aluminium sulphate ($Al_2(SO_4)_3$) of 37 g/l; anodic current density of 2.5 A/dm^2; anodic layer growth rate of 0.5 – 2.0 µm/min; and electrolyte temperature of 4 ± 2 °C.

The chromium coating was deposited by electroplating. Chromium plating was performed at 55 – 60 °C with a current density of 30 – 40 A/dm^2 and an anode-to-cathode surface area ratio of 2:1, for 8 – 9 hours. The electrolyte contained 225 – 250 g/l chromium trioxide (CrO_3, Cr^{6+}), 2.0 – 2.9 g/l sulfuric acid (H_2SO_4), up to 12 g/l trivalent chromium (Cr^{3+}) and up to 8 g/l iron (Fe^{2+}/Fe^{3+}). Three-component Pb-Sb-Sn anodes (81 – 86 % Pb, 4 % Sb, 10 – 15 % Sn) were used to ensure stable anodic performance. Trivalent chromium stabilises the bath and regulates redox equilibrium, while iron ions improve coating uniformity and adhesion.

The phase composition of the deposited coatings was investigated by X-ray diffraction (XRD) analysis using CuKα radiation (λ = 1.54242 Å). The measurements were conducted with a Philips PW1050 diffractometer equipped with a PW1830 generator operating at 45 kV and 40 mA. A Fe filter was used to reduce fluorescence, and scans were performed in step mode with a scanning speed of 4 °/min, a step size of Δ2Θ = 0.2° and a dwell time of 15 s per degree. The substrate materials were carefully selected to minimise signal interference, i.e. they do not exhibit diffraction peaks overlapping with those of the coatings.

The texture coefficient P(hkl) of the coatings was calculated according to the Harris method for cubic crystal systems [19]. This coefficient provides critical insights into the crystallographic orientation and is directly related to key mechanical properties such as hardness and strength. It serves as a predictive indicator for assessing the coating performance under operational conditions.

The chemical composition and elemental distribution of the coatings were quantitatively analysed to determine the principal elements and their respective concentrations, expressed as weight percentage (wt. %). Energy-dispersive X-ray spectroscopy (EDS) was carried out using a Hirox SH-5500P scanning electron microscope equipped with a Bruker QUANTAX 100 advanced X-ray microanalysis system. The analysis was conducted at two locations: the top surface and the cross-section surface of the coating.

The composition of the coatings was determined under the following conditions: for

anodic oxide (Al-based) coating, analysis focused on predefined elements Al, O and S; and for chromium (Cr-based) coating, analysis focused on predefined elements Fe, Cr, O and S. All identified chemical elements were included by default.

Samples with oxide and chromium coatings, measuring 20 mm in diameter and 10 mm in height, were examined. The samples were prepared according to a standard procedure, including wet grinding using abrasive papers of successive grades (P250, P400, P600, P800, P2000, P2400 and P4000) and mechanical polishing with diamond paste on a Leco PX300 modular polishing machine. The tests were performed at an ambient temperature of 23.9 °C. For the aluminium alloy EN AW-7075 with a hard anodised oxide coating, the microstructure was revealed by etching in a 0.5 % aqueous solution of hydrogen fluoride (HF). Coating thicknesses were determined as the arithmetic mean of ten measurements.

3. Results and discussion

3.1 XRD analysis

The obtained XRD patterns (Figs. 1 and 2) depict the intensity *I* in imp/s as a function of the diffraction angle 2Θ in °. The noticed peaks correspond to characteristic crystallographic planes of the constituent phases, providing conclusive evidence for the successful formation of anodic oxide and chromium coatings.

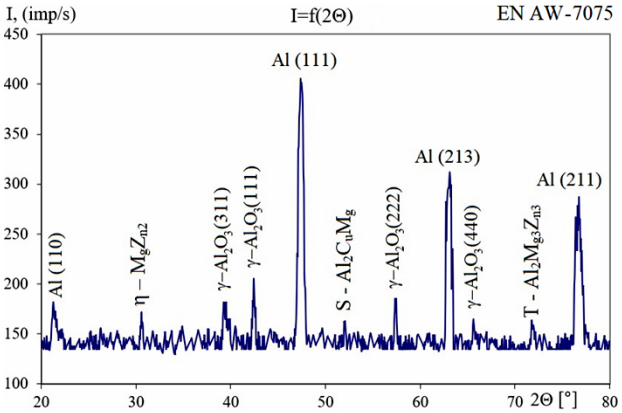

Figure 1. XRD pattern of anodic oxide coating

The XRD analysis revealed that the hard anodic oxide coating predominantly consists of aluminium (Al) and the γ-phase of aluminium oxide (γ-Al_2O_3). Additionally, minor diffraction peaks corresponding to secondary intermetallic phases S (Al_2CuMg), T ($Al_2Mg_3Zn_3$) and η ($MgZn_2$), were also detected (Fig. 1). These S, T and η phases refer to secondary intermetallic precipitation phases characteristic of high-strength aluminium alloys of the Al-Zn-Mg-Cu system (e.g. EN AW-7075): S phase increases strength, T phase is stable phase after prolonged ageing and η phase is dominant precipitation phase responsible for main precipitation hardening effect. The diffraction angles of these phases are in close agreement with theoretical values, indicating that the coating exhibits a near-stoichiometric composition. The presence of the S, T and η phases is primarily attributed to the influence of the substrate material, as these are not characteristic of pure anodic layers. The sharp and narrow XRD peaks further indicate that the coating structure is homogeneous and exhibits a coarse-grained morphology.

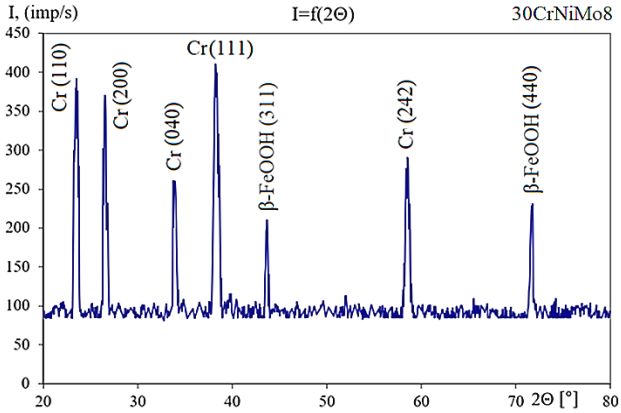

Figure 2. XRD pattern of chromium coating

Due to the relatively low coating thickness of approximately 28 µm, the XRD spectrum shows only four distinct peaks, all of which are associated with the aluminium phase. These peaks are well-defined and exhibit texturing, occurring at the following diffraction angles: 2Θ = 46.95 – 47.85°, textured along the <111> direction; 2Θ = 20.80 – 22.35°, textured along the <110> direction; 2Θ = 76.25 – 77.10°, textured along the <211> direction; and 2Θ = 62.65 – 63.45°, textured along the <213> direction. For the γ-phase of Al_2O_3, the main peaks are as follows: 2Θ = 42.15 – 42.70°, textured along the <111> direction; 2Θ = 57.15 – 57.70°, textured along the <222> direction; and 2Θ = 39.05 – 39.95°, textured along the <311> direction; and 2Θ = 65.35 – 66.15° textured along the <440> direction. Due to the relatively low deposition temperature, the dominant crystallographic orientation noticed in the XRD pattern corresponds to the <111> direction, which is characteristic of a face-centred cubic (FCC) crystal structure.

In the XRD pattern of the chromium coating (Fig. 2), distinct peaks associated with metallic

chromium (Cr) and goethite (β-FeOOH) were identified. The absence of substrate-related reflections is attributed to the substantial coating thickness, which effectively prevents X-ray penetration into the underlying material during the diffraction process. The principal diffraction peaks corresponding to metallic chromium are well defined and occur at the following diffraction angles: 2Θ = 37.75 – 38.90°, textured along the <111> direction; 2Θ = 23.10 – 23.95°, textured along the <110> direction; 2Θ = 26.15 – 26.90°, textured along the <200> direction; 2Θ = 33.65 – 34.25°, textured along the <040> direction; and 2Θ = 58.00 – 59.05°, textured along the <242> direction. For goethite, the main peaks are as follows: 2Θ = 43.40 – 44.05°, textured along the <311> direction; and 2Θ = 71.30 – 72.05°, textured along the <440> direction. The identified crystallographic orientations correspond to the <111>, <110>, <200>, <040>, <242>, <311> and <440> directions. As noticed in the anodic oxide coating, the dominant orientations are <111> and <110>, which are characteristic of a face-centred cubic (FCC) lattice structure.

The obtained results are in agreement with data reported by other authors, thereby confirming both the reliability of the experimental findings and the validity of the applied research methodology [20,21]. These observations are in agreement with previously reported studies on anodised Al 7075 and chromium coatings, supporting the correlation between texture coefficients and enhanced mechanical and corrosion properties [22,23]. Figure 3 illustrates the texture coefficients P(hkl) for both the anodised oxide and chromium coatings.

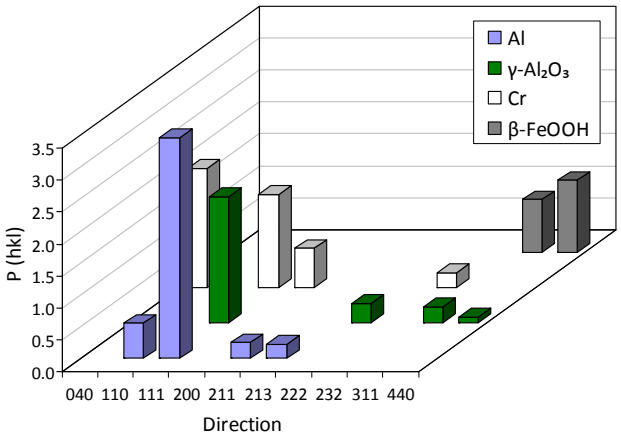

Figure 3. Texture coefficient P(hkl)

The texture coefficients specifically for the Al phase are shown in Table 1. However, the table also includes results for the γ-Al_2O_3 phase. For the chrome coating, the texture coefficients for the Cr phase are shown in Table 2, together with the corresponding results for the β-FeOOH phase. These findings substantiate that both coatings possess pronounced crystallographic textures, which directly enhance their mechanical performance and corrosion resistance. These values indicate the crystallographic orientation of the phases within the coatings. Higher texture coefficients, particularly in the <111> and <110> directions in the anodised coating, suggest a pronounced preferential orientation, which enhances mechanical properties such as hardness and wear resistance. A similar trend is noticed in the chromium coating, reaffirming their superior performance and durability.

Table 1. Texture coefficients for phases of the anodised oxide coating

Phase	Crystal orientation (hkl)	Texture coefficient P(hkl)
Al	<111>	3.45
	<110>	0.55
	<211>	0.25
	<213>	0.23
γ-Al_2O_3	<111>	1.97
	<222>	0.30
	<311>	0.26
	<440>	0.10

Table 2. Texture coefficients for phases of the chromium coating

Phase	Crystal orientation (hkl)	Texture coefficient P(hkl)
Cr	<111>	1.45
	<110>	0.48
	<200>	0.61
	<040>	1.86
	<242>	0.23
β-FeOOH	<311>	0.82
	<440>	1.21

The textures along the <111> and <040> directions are most prominent. While the <111> orientation is predominantly associated with aluminium phases, the <040> orientation is associated with higher hardness and improved corrosion resistance. The elevated texture coefficient values reflect a strong crystallographic

texture in these directions. The presence of sharply defined diffraction peaks confirms the existence of well-aligned crystal structures. This pronounced texturing significantly improves mechanical performance, particularly in chromium-based coating, making it suitable for applications requiring enhanced resistance to wear and corrosion.

3.2 Chemical composition and elemental distribution

The results of the anodic oxide coating tests are illustrated in Figures 4 – 8. Figure 4 shows a cross-section surface of the anodic oxide coating with dimension markings.

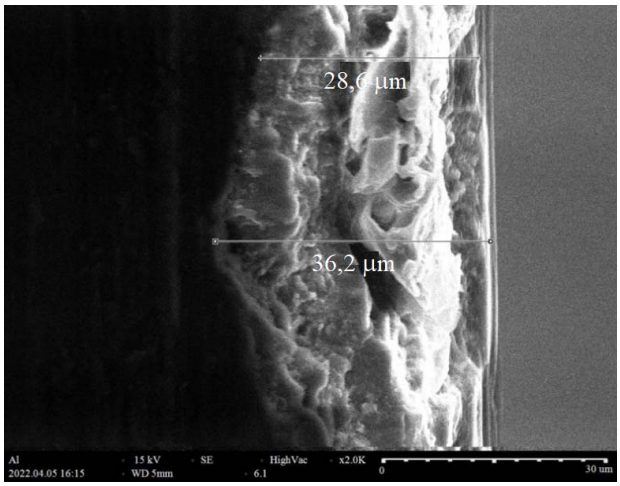

Figure 4. Cross-section surface of the anodic oxide coating

Figure 5 presents the EDS analysis conducted on the top surface of the anodic oxide coating within the designated area, focusing on the predefined elements Al, O and S. The corresponding chemical composition (wt. %), along with the elemental spectrum, is presented in Figure 6.

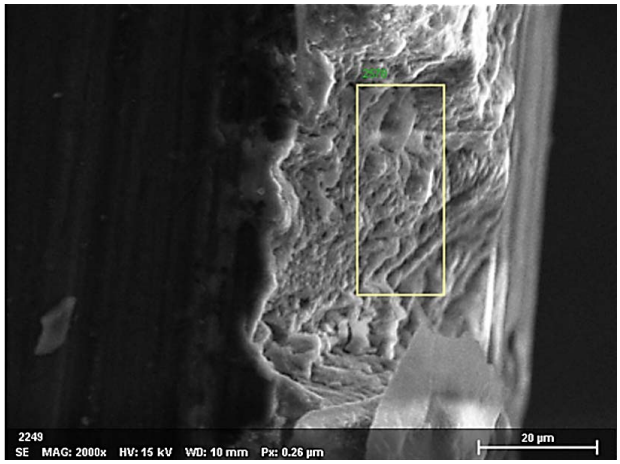

Figure 5. EDS analysis of the top surface of the anodic oxide coating

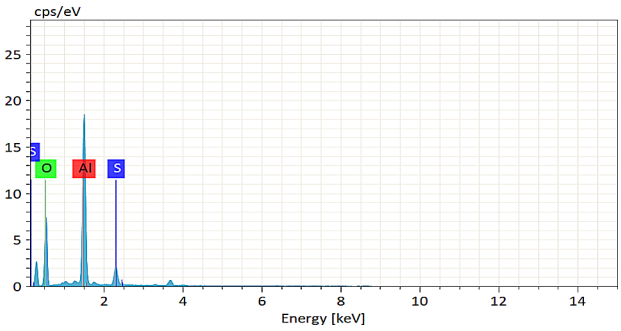

Element	Atomic number	Netto	Mass, %	Normalised mass, %	Absolute error, %	Relative error, %
O	8	24,685	28.44	46.61	3.59	12.63
Al	13	74,773	28.22	46.24	1.34	4.74
S	16	9849	4.36	7.15	0.19	4.33

Figure 6. EDS analysis of the anodic oxide coating top surface, focusing on predefined elements Al, O and S

The results of the EDS analysis of the anodic oxide coating top surface within the specified area, encompassing all detected chemical elements, along with the corresponding spectrum, are shown in Figure 7.

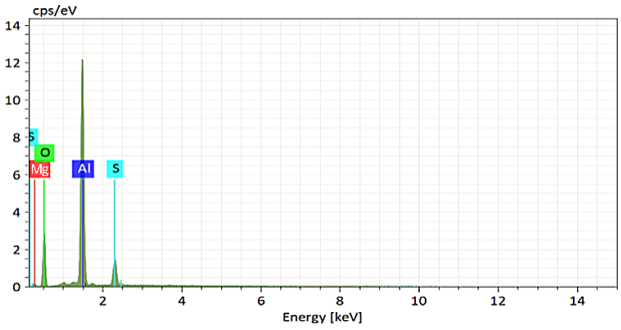

Element	Atomic number	Netto	Mass, %	Normalised mass, %	Absolute error, %	Relative error, %
Al	13	52,660	40.48	49.05	1.91	4.73
O	8	9802	28.79	34.89	4.07	14.13
Mg	12	621	7.36	8.92	1.94	26.39
S	16	7096	5.89	7.14	0.25	4.27

Figure 7. EDS analysis of the anodic oxide coating top surface, including all identified chemical elements

The recorded spectra reveal the elements constituting the coating, predominantly aluminium and oxygen. Due to the relatively small thickness of the anodic oxide coating, elements originating from the substrate, such as magnesium, are also detected. This discrepancy may be attributed to either preliminary electrochemical high-amperage oxidation of the aluminium alloy or a localised measurement of an area containing insufficiently dissolved zinc (a zinc agglomerate or cluster) formed during the solid phase precipitation of T ($Al_2Mg_3Zn_3$) and η ($MgZn_2$). The presence of sulphur can be explained by the active influence of the electrolyte composition, which includes sulfuric acid (H_2SO_4) and aluminium sulfate ($Al_2(SO_4)_3$).

The results of the EDS analysis of the anodic oxide coating cross-section surface, focusing on predefined elements (Al, O and S), are provided in Figure 8. The chemical compositions measured on the coating top surface are consistent with those noticed on the cross-section surface. This uniformity confirms the reliability of the hard anodising process parameters and demonstrates uniform deposition of the coating.

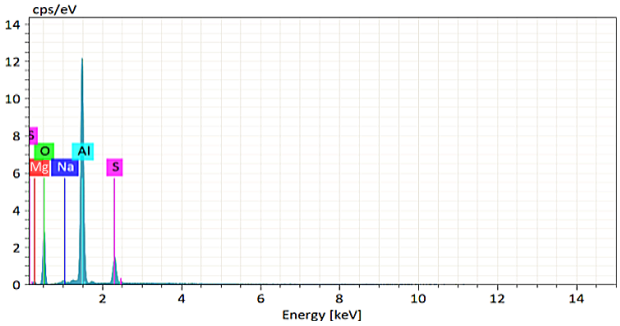

Element	Atomic number	Netto	Mass, %	Normalised mass, %	Absolute error, %	Relative error, %
Al	13	34,453	39.61	55.56	1.88	4.76
O	8	6422	25.75	36.11	3.88	15.09
S	16	4712	5.94	8.33	0.26	4.42

Figure 8. EDS analysis of the anodic oxide coating cross-section surface, focusing on predefined elements Al, O and S

The results of the tests on chromium coating are presented in Figures 9 – 13. Figure 9 shows a cross-section surface of the chromium coating with dimension markings.

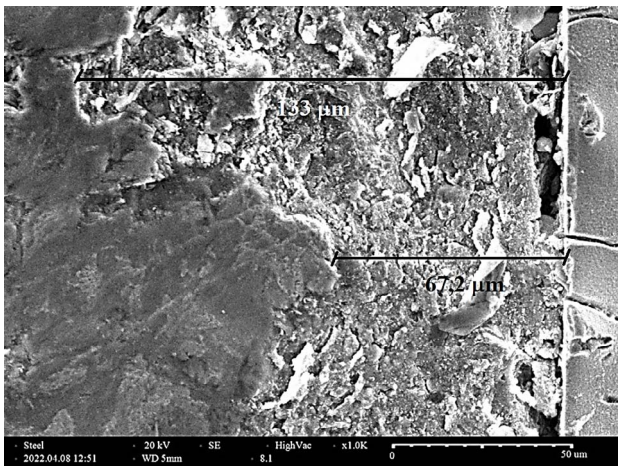

Figure 9. Cross-section surface of the chromium coating

The top surface of the chromium coating was analysed by EDS, with emphasis on the predefined elements Fe, Cr, O and S (Fig. 10). The results of the EDS analysis of the chromium coating top surface, including all detected chemical elements, along with the corresponding spectrum, are shown in Figure 11.

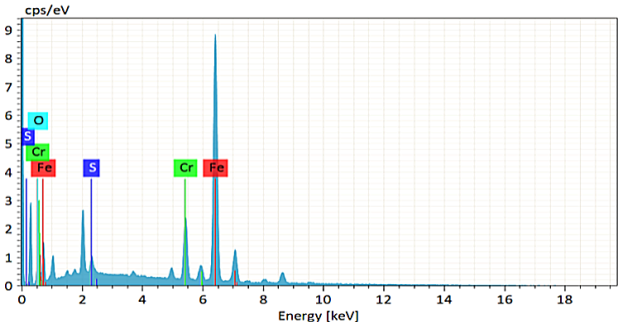

Element	Atomic number	Netto	Mass, %	Normalised mass, %	Absolute error, %	Relative error, %
Fe	26	88,086	48.97	80.15	1.33	2.72
Cr	24	19,866	7.19	11.76	0.23	3.15
O	0	5726	4.03	6.59	0.64	15.91
S	16	3599	0.91	1.49	0.06	6.91

Figure 10. EDS analysis of the chromium coating top surface, focusing on predefined elements Fe, Cr, O and S

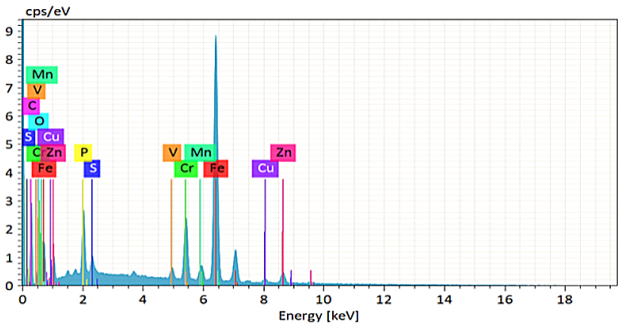

Element	Atomic number	Netto	Mass, %	Normalised mass, %	Absolute error, %	Relative error, %
Fe	26	85,695	40.41	47.52	1.10	2.73
C	6	11,086	21.60	25.40	3.01	13.91
O	8	6492	6.37	7.49	0.98	15.36
Cr	24	19,957	6.12	7.20	0.20	3.21
Zn	30	4069	3.78	4.45	0.15	3.89
P	15	13,277	2.93	3.44	0.14	4.90
Mn	25	2667	1.03	1.21	0.06	5.86
Cu	29	1273	1.02	1.20	0.07	6.56
V	23	3321	0.95	1.12	0.06	5.99
S	16	3942	0.82	0.96	0.06	7.19

Figure 11. EDS analysis of the chromium coating top surface, including all identified chemical elements

The results of the EDS analysis of the chromium coating cross-section surface are consistent with those from the top surface. Figure 12 shows the results focusing on predefined elements, and Figure 13 shows the results including all identified chemical elements.

One notable difference is the low concentration of Fe atoms in the cross-section surface of the coating analysis. Elemental distribution across the coating thickness indicates that chromium concentrations are highest near the coating surface, while carbon concentrations are elevated close to the substrate. This pattern likely reflects

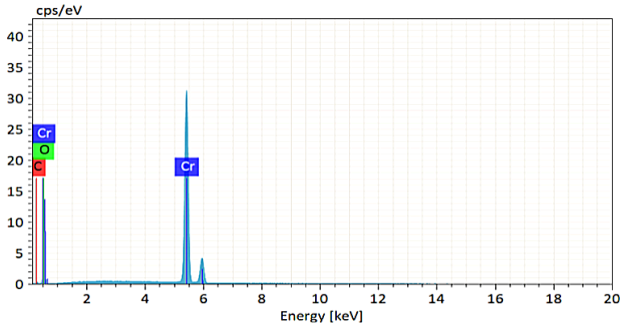

Element	Atomic number	Netto	Mass, %	Normalised mass, %	Absolute error, %	Relative error, %
Cr	24	237,890	84.08	95.28	2.28	2.72
O	8	4202	2.12	2.40	0.37	17.35
C	6	1232	2.04	2.31	0.46	22.62

Figure 12. EDS analysis of the chromium coating cross-section surface, focusing on predefined elements Cr, O and S

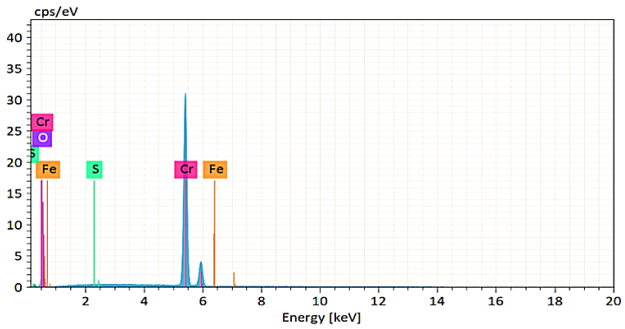

Element	Atomic number	Netto	Mass, %	Normalised mass, %	Absolute error, %	Relative error, %
Cr	24	214,969	84.92	97.60	2.31	2.72
O	8	3800	2.02	2.33	0.36	17.72
S	16	164	0.05	0.06	0.03	59.05
Fe	26	22	0.02	0.02	0.00	21.90

Figure 13. EDS analysis of the chromium coating cross-section surface, including all identified chemical elements

deposition process and sample preparation effects, rather than actual diffusion. Noticed Fe content may result from minor contamination during cross-sectional analysis. These findings are consistent with the expected behaviour for coatings deposited at low temperatures under the applied electrochemical conditions.

3.3 Metallographic analysis and thickness

Figure 14a shows the microstructure of hard anodised oxide coating on the aluminium alloy 7075 substrate (Fig. 14b). The sample surface shows a dark coating with good adhesion to the substrate. The substrate microstructure comprised elongated grains of the solid solution of copper and zinc in aluminium and polygonal crystals of the S phase (Al_2CuMg). Dark, rounded precipitates of the T phase ($AlMg_3Zn_3$) and the η phase ($MgZn_2$) were also noticed.

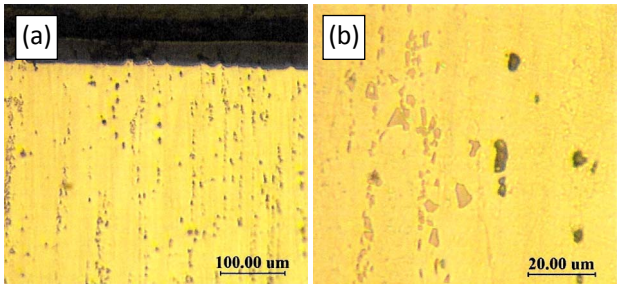

Figure 14. Microstructure of: (a) hard anodised oxide coating and (b) substrate

The microstructure of the steel sample with the chromium coating was revealed using a 4 % solution of nitric acid (HNO_3) in ethyl alcohol. The coating is presented in Figure 15a. The steel surface exhibited a bright coating with good adhesion to the substrate, consisting mainly of metallic chromium, with minor oxides formed during deposition, along with inclusions of goethite (β-FeOOH). The microstructure of the steel substrate included martensite and rounded carbide precipitates, as shown in Figure 15b. The chromium coating on the steel sample was approximately ten times thicker than the anodised oxide coating, measuring 288.98 ± 1.58 µm.

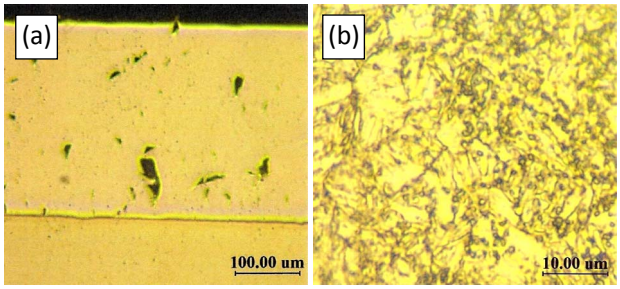

Figure 15. Microstructure of: (a) chromium coating and (b) substrate

Metallographic analysis confirmed the microstructural features of both coatings, i.e. a hard anodised oxide coating on aluminium and a chromium coating on steel, showing metallic phases and minor oxides, which is entirely consistent with the XRD results.

4. Conclusion

Based on the conducted research and the reported results regarding the operational and technological characteristics of the obtained coatings, the following important conclusions can be drawn.

Anodised oxide coating on aluminium and chromium coating on steel were successfully obtained by electrochemical anodic and cathodic deposition methods, respectively.

The results of the X-ray structural analysis of the anodised oxide coating show predominant phases of Al and the γ-phase of Al_2O_3, along with less pronounced phases such as S phase (Al_2CuMg), T phase ($Al_2Mg_3Zn_3$) and η phase ($MgZn_2$). The phase peaks correspond closely to theoretical values, confirming the near-stoichiometric composition of the coating.

The X-ray diffractogram of the chromium coating reveals only phases of metallic chromium and minor oxides, along with goethite (β-FeOOH). This is attributed to the substantial thickness of the coating of 288.98 μm, which prevents the substrate material from influencing the diffraction results. The coating thickness also contributes to enhanced substrate protection, improving wear and corrosion resistance under operational conditions.

High texture coefficients indicate a strong preferred crystallographic orientation, which will correlate with enhanced mechanical properties such as hardness and wear resistance.

Metallographic analysis confirmed the hypothesis suggested by the X-ray structural and chemical analyses, showing that the microstructure of the anodised oxide coating comprises elongated grains of a solid solution of copper and zinc in aluminium, polygonal crystals of the S phase (Al_2CuMg), dark, rounded precipitates of the T phase ($Al_2Mg_3Zn_3$) and fine precipitates of the η phase ($MgZn_2$).

Acknowledgement

The authors would like to thank the Research and Development Sector at the Technical University of Sofia for the financial support. The authors also wish to thank Arsenal JSC – Kazanlak for the financial support, which enabled the present research.

References

[1] E. Razzouk, D. Koncz-Horváth, T.I. Török, Critical challenges in the anodizing process of aluminium-silicon cast alloys – A review, Crystals, Vol. 14, No. 7, 2024, Paper 617, DOI: 10.3390/cryst14070617

[2] W. Lee, The anodization of aluminum for nanotechnology applications, JOM, Vol. 62, No. 6, 2010, pp. 57-63, DOI: 10.1007/s11837-010-0088-5

[3] Z.B. Yang, J.C. Hu, K.Q. Li, S.Y. Zhang, Q.H. Fan, S.A. Liu, Advances of the research evolution on aluminum electrochemical anodic oxidation technology, IOP Conference Series: Materials Science and Engineering, Vol. 283, 2017, Paper 012003, DOI: 10.1088/1757-899X/283/1/012003

[4] F. Hekmat, B. Sohrabi, M.S. Rahmanifar, A. Jalali, Electrophoretic deposition of multi-walled carbon nanotubes on porous anodic aluminum oxide using ionic liquid as a dispersing agent, Applied Surface Science, Vol. 341, 2015, pp. 109-119, DOI: 10.1016/j.apsusc.2015.02.142

[5] H. Masuda, K. Fukuda, Ordered metal nanohole arrays made by a two-step replication of honeycomb structures of anodic alumina, Science, Vol. 268, No. 5216, 1995, pp. 1466-1468, DOI: 10.1126/science.268.5216.1466

[6] Z. Zhang, S. Sridhar, G. Wei, Y. Yu, Z. Zhang, L. Jiang, Y. Yang, M.W. Shahzad, X. Chen, B.B. Xu, A highly controlled fabrication of porous anodic aluminium oxide surface with versatile features by spatial thermo-anodization, Surface and Coatings Technology, Vol. 408, 2021, Paper 126809, DOI: 10.1016/j.surfcoat.2020.126809

[7] M.M. Lohrengel, K.P. Rataj, T. Münninghoff, Electrochemical machining – Mechanisms of anodic dissolution, Electrochimica Acta, Vol. 201, 2016, pp. 348-353, DOI: 10.1016/j.electacta.2015.12.219

[8] M. Bedolla-Hernández, G. Rosano-Ortega, F.J. Sánchez-Ruiz, J. Bedolla-Hernández, P.S. Schabes-Retchkiman, C.A. Vega-Lebrún, Electrodeposition mechanism of chromium nanoparticle coatings: Modeling and experimental validation, Chemical Engineering Science, Vol. 252, 2022, Paper 117291, DOI: 10.1016/j.ces.2021.117291

[9] F.I. Danilov, V.S. Protsenko, T.E. Butyrina, E.A. Vasil'eva, A.S. Baskevich, Electroplating of chromium coatings from Cr(III)-based electrolytes containing water soluble polymer, Protection of Metals, Vol. 42, No. 6, 2006, pp. 560-569, DOI: 10.1134/S0033173206060075

[10] V.S. Protsenko, L.S. Bobrova, A.S. Baskevich, S.A. Korniy, F.I. Danilov, Electrodeposition of chromium coatings from a choline chloride based ionic liquid with the addition of water, Journal of Chemical Technology and Metallurgy, Vol. 53, No. 5, 2018, pp. 906-915.

[11] V. Gilhotra, R. Yadav, A. Sugha, L. Das, A. Vashisht, R. Bhatti, M.S. Bhatti, Electrochemical treatment of high strength chrome bathwater: A comparative study for best-operating conditions, Cleaner Engineering and Technology, Vol. 2, 2021, Paper 100093, DOI: 10.1016/j.clet.2021.100093

[12] I. Ali, M.M. Quazi, E. Zalnezhad, A.A.D. Sarhan, N. Liana Sukiman, M. Ishak, Hard anodizing of aerospace AA7075-T6 aluminum alloy for improving surface properties, Transactions of the Indian Institute of Metals, Vol. 72, No. 10, 2019, pp. 2773–2781, DOI: 10.1007/s12666-019-01754-5

[13] F. Guo, Y. Cao, K. Wang, P. Zhang, Y. Cui, Z. Hu, Z. Xie, Effect of the anodizing temperature on microstructure and tribological properties of 6061 aluminum alloy anodic oxide films, Coatings, Vol. 12, No. 3, 2022, Paper 314, DOI: 10.3390/coatings12030314

[14] R. Singleton, E. Singleton, Fundamentals of barrel plating, Metal Finishing, Vol. 109, No. 8, 2011, pp. 14-22, DOI: 10.1016/S0026-0576(13)70035-7

[15] C. Conev, T. Karadzhov, Application of the finite element method for the design of small arm barrels, Environment. Technology. Resources, Vol. 14, No. 2, 2023, pp. 114-118, DOI: 10.17770/etr2023vol2.7213

[16] K. Wang, Z. Wang, Y. Wu, Y. Xia, Y. Xun, F. Wu, J. Jiao, L. Du, Calculation of resonance fluorescence scattering cross sections of metal particles in the middle and upper atmosphere and comparison of their detectability, Atmosphere, Vol. 14, No. 8, 2023, Paper 1283, DOI: 10.3390/atmos14081283

[17] S. Yavuz, Y. Sert, M. Karsli, T. Küçükömeroğlu, Determining optimum anodic oxidation parameters for hardness and wear properties of AA7075-T6 alloys using Taguchi design, Brilliant Engineering, Vol. 2, No. 1, 2021, pp. 10-17, DOI: 10.36937/ben.2021.001.003

[18] R. Bertolini, E. Simonetto, L. Pezzato, A. Fabrizi, A. Ghiotti, S. Bruschi, Mechanical and corrosion resistance properties of AA7075-T6 sub-zero formed sheets, The International Journal of Advanced Manufacturing Technology, Vol. 115, No. 9-10, 2021, pp. 2801-2824, DOI: 10.1007/s00170-021-07333-7

[19] D. Roman, J.C. Bernardi, C.D. Boeira, F.S. de Souza, A. Spinelli, C.A. Figueroa, R.L.O. Basso, Nanomechanical and electrochemical properties of ZrN coated NiTi shape memory alloy, Surface and Coatings Technology, Vol. 206, No. 22, 2012, pp. 4645-4650, DOI: 10.1016/j.surfcoat.2012.05.039

[20] B. Kościelniak, D. Groch, W.J. Nowak, M. Drajewicz, P. Kwolek, Microstructure and corrosion resistance of 7075 aluminium alloy composite material obtained from chips in the high-energy ball milling process, Materials, Vol. 17, No. 21, 2024, Paper 5331, DOI: 10.3390/ma17215331

[21] E. Broitman, A. Jahagirdar, E. Rahimi, R. Meeuwenoord, J. M.C. Mol, Microstructural, nanomechanical, and tribological properties of thin dense chromium coatings, Coatings, Vol. 14, No. 12, 2024, Paper 1597, DOI: 10.3390/coatings14121597

[22] D. Kusmič, L. Klakurková, M. Julis, P. Gejdoš, J. Vilis, O. Cech, The corrosion resistance of hard anodised EN AW 7075 T6 alloy, ECS Transactions, Vol. 105, 2021, Paper 329, DOI: 10.1149/10501.0329ecst

[23] S. Sun, Z. Wu, M. Pang, J. Chang, Y. Xuan, H. Qi, R. Yang, Y. Wu, Microstructure and corrosion behavior of chromium-rich stainless steel coatings deposited by different laser cladding processes, Journal of Materials Research and Technology, Vol. 29, 2024, pp. 3879-3890, DOI: 10.1016/j.jmrt.2024.02.044